Research Article
Open Access

# Evaluating the effects of titanium dioxide (TiO2) and carbon-nanofibers (CNF) as cement partial replacement on concrete properties

## Abstract

The objective of this study is to develop durability and mechanical characteristics of concrete mixtures by incorporating nano-engineering practices. The application of titanium dioxide ($TiO_2$) and carbon-nanofibers (CNF) in concrete have received strong consideration in recent years. However, the durability and mechanical properties of these kinds of concretes have not been evaluated thoroughly. To achieve this purpose, an experimental program was designed to assess the performance of $TiO_2$ and CNF singularly and simultaneously. The mechanical and durability-related characteristics of concrete containing $TiO_2$ and CNF have been investigated. These nanoparticles as a partial replacement of cement might develop the pore structure of concrete leading to improved durability and strength upgrading of the concrete. The slump flow test was carried out to evaluate the capabilities of $TiO_2$ and CNF in the slump retention. To evaluate abrasion resistance and wear-ability of samples, weight loss, and rut depths were measured, respectively. Also, the resistance to freezing/thawing, bulk electrical resistivity, and shrinkage test were performed to analyze the pore structure. Although $TiO_2$ and CNF would fill gel pores of the paste to improve pore structure, using too much weaken mechanical characteristics.

**Keywords:** concrete, $TiO_2$, CNF, nanoparticle, microstructure, strength, durability, pore

Volume 4 Issue 1 - 2018

Alireza Joshaghani
Zachry Department of Civil Engineering, Texas A&M University, USA

**Correspondence:** Alireza Joshaghani, Ph.D. Candidate, Zachry Department of Civil Engineering, Texas A&M University, 1800 Holleman Drive Apt 1210, USA, Email joshaghani@tamu.edu

**Received:** December 21, 2017 | **Published:** January 30, 2018

**Abbreviations:** CNF, carbon-nanofibers; HWT, hamburg-wheel-track; LVDT, linear variable differential transformer; SEM, scanning electron microscopy; HRWR, high range water reducer; OPC, ordinary portland cement; w/c, water/cement

## Introduction

Many scientists and engineers are now looking for the right key for designing sustainable infrastructure systems that show higher durability and have a long maintenance-free performance with low repair costs. In other words, enhancing built infrastructure service life will lessen the demand for new infrastructure, resulting in little raw materials usage, less energy consumption, and reduction of $CO_2$ emission. From the materials point of view, the effort to increase the service life of infrastructure can be made by using various advanced high-quality materials including the newly emerging concepts of multifunctional structural materials. Synthetic nanomaterials are being utilized for numerous applications in the construction and infrastructure industries. The opportunities for application of nano-engineering in developing concrete mixtures applications are immense. The usage of nanomaterials in evolving mix designs should be deliberated not only for improving material properties, but also in the perspective of energy conservation and durability issues. Areas of improvement through nano-engineering and other novel approaches have been evaluated. This development affected mechanical performance (e.g., high strength through the formation of a denser microstructure with high C-S-H [stiffer] content and low C-H content, and improvement in ductility and toughness). Moreover, durability (e.g., reduction in shrinkage, reduction in permeability, reduction in leaching potential, and an increase in abrasion resistance) of the materials for overlay and other thin topical applications in pavements and bridges has been promoted.

The addition of conductive fillers such as carbonaceous nanomaterials (e.g., CNFs) to conventional concrete composite causes the concrete to become electrically conductive. In electrically conductive concrete, damage can be monitored by measuring the change of electrical resistivity generated by micro-deformation or change of connectivity of the conduction path under an external load (analysis of the strain or stress variations in the structure member). The practical application of these phenomena is a real-time detection of damage in concrete structures and snow and ice removal with straightforward and inexpensive electrical equipment.[1–3] Other benefits of adding both steel fiber and CNF are the enhancement of mechanical strength, crack resistance properties, and reduction in permeability/resistance to chemical attack, which produces more durable concrete. A combined effect of all the benefits enables a conventional concrete to acquire multifunctional climate-adaptive behavior and can be used in bridge deck topical applications. The performance of concrete with $TiO_2$ has been examined. The greater extent of the abrasion resistance of concrete is reduced by incorporating more $TiO_2$ nanoparticles.[4,5] Photo catalysis particles of $TiO_2$ can be used to purify the air with concrete pavement surfaces. This technology is principally helpful for urban infrastructures where traffic volume develops rapidly. There are different methods to incorporate $TiO_2$ into cementitious materials such as mixing during cement making, suspension solution onto cementitious matrix surface, or sprinkling onto fresh cementitious material's surface.[6] All of these methods could implement the photo catalytic effects; however, the efficiency and long-term performance remain challenging because of hydration reactions, $TiO_2$ effective surface area reduction, and poor dispersibility.[7,8] Using $TiO_2$ with cementitious mortar mixture as a thin layer over the concrete pavement surface has a potential to support environmentally friendly road infrastructure and the durability. However, resistance to wear of

$TiO_2$ surface coating has not been evaluated comprehensively, which might be a serious obstacle preventing the large-scale application of this technology.[9] In fact, the nano-sized particles may be removed by traffic and harsh service conditions.[10]

The areas of application of nano-engineering to develop environmentally in a friendly way and multifunctional materials (mixes) for repair and thin overlay applications will be identified. The information about the most efficient nanomaterials and their combination and dosage to achieve the set of performance/properties are determined. It is possible that a mix of different types of nanomaterials instead of one single nanomaterial will be more efficient to achieve multifunctional behavior. A combination of $TiO_2$ and CNF will be very useful to increase mechanical behavior, increase crack resistance property, add self-cleaning and de-polluting properties due to photo catalytic action, increase abrasion resistance property, and increase conductivity. CNFs might act as supporting materials with high surface areas, catalysts for the reduction reaction, and efficient electron-transfer mediators.[11–14] CNFs provide spatial confinement for $TiO_2$ and large surface areas that increase the rates of redox reactions. It may help the graphene surface to improve photo catalytic water splitting by enhancing the light absorption of $TiO_2$. These nanomaterials have useful characteristics, including relatively simple fabrication, cost-effectiveness, and flexibility.[15,16] Generally, CNFs in a thin layer have many advantages with photo catalytic materials, since they have large surface areas and excellent conductivities.[17–20] One of the characteristics of CNFs is that they have a complex structure. Their exterior surface, typically consists of conically shaped graphite planes canted with respect to the longitudinal fiber axis. These edges help the fiber in the matrix and prevent interfacial slip. The feasibility of using topical materials is ascertained based on the characteristics of the materials involved to satisfy both fresh and hardened concrete requirements. In this study, durability and other mechanical properties of $TiO_2$ with the application of CNFs are investigated.

## Experimental program

An experimental design is developed based on a step-by-step approach: selection of a nano-engineering approach (CNF and $TiO_2$) to achieve the target performance properties, followed by identifying relevant factors and their levels based on data collected from the literature review.

### Materials

For all samples, the cementitious material Type I ordinary Portland cement (OPC) conforming to the requirements of ASTM C150 was used.[21] The physical characteristics and chemical compositions of the Portland cement and $TiO_2$ nanoparticles are summarized in Table 1 & 2, respectively. Moreover, the coarse aggregate size number was 57 (25.0 to 4.75 mm) according to ASTM C33.[22] Also, fine aggregate met the specifications mentioned in ASTM C33 standard. In all mixtures, to increase the workability of the mixtures, super plasticizer was added, which was a polycarboxylate-based high range water reducer (HRWR) agent with the density of 1.03-1.05 g/cm$^3$ (at 20°C). The highly graphitic carbon nanofibers with the following characteristics were used: 45 m$^2$/g surface area with 1.6 g/cm$^3$ density. The CNFs were manufactured using the chemical decomposition of principally natural gas over an iron-sulfide catalyst in a reactor maintained near 1100°C. This process happens with quick heating at around 600°C and does not change the nanofiber's structure. The fibers with a diameter of 100 nm showed a tensile strength and modulus of 6 and 600 Gpa, respectively. The length ranges of 30–100 are used. These nanofiber has been subjected to a typical debulking process. CNF was prepared in amounts of 0.1-0.5 wt. % of cement. CNFs have a complex microstructure. The exterior surface of this nano-fiber characteristically involves of conically shaped graphite planes canted with respect to the longitudinal fiber axis. It might help the fiber to not interfacial slip in the matrix. The Scanning Electron Microscopy (SEM) picture of the fibers can be seen in Figure 1. The outer walls are the thin lines on the surface of the nanofiber.

**Table 1** Chemical composition and physical properties of cement

| Chemical analysis (weight %) | Cement |
|---|---|
| $SiO_2$ | 21.56 |
| $Al2O_3$ | 6.67 |
| $Fe_2O_3$ | 6.17 |
| CaO | 49.88 |
| MgO | 4.51 |
| $SO_3$ | 2.75 |
| $K_2O$ | 0.76 |
| $Na_2O$ | 0.43 |
| LOI | 2.79 |
| Specific gravity (g/cm$^3$) | 3.18 |
| Specific surface area (cm$^2$/g) | 4168 |

**Table 2** Properties of $TiO_2$ nanoparticles

| Diameter (nm) | Surface volume ratio (m$^2$/g) | Density (g/cm$^3$) | Purity (%) |
|---|---|---|---|
| 22 ± 2 | 163 | 0.14 | >99.9 |

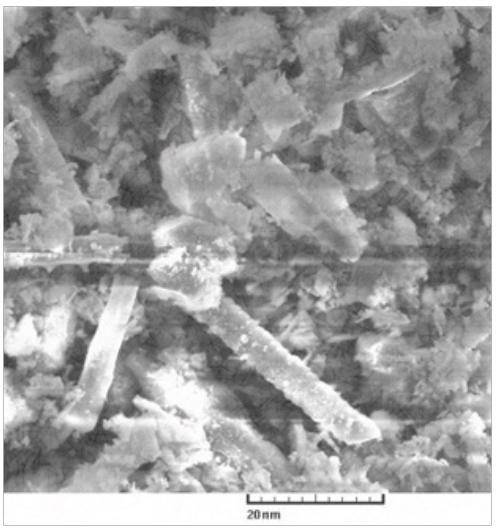


**Figure 1** SEM image of the exterior of a cementitious nanocomposite with CNF.

### Mixture design

A number of nine concrete mixtures were designed with a certain water/cement (w/c) ratio of 0.45 and a binder content of 450 kg/m$^3$. Concrete mixtures were fabricated with 0.2 and 0.4 wt% of cement

replacement by CNF, and 3 and 5 wt% of cement replacement by $TiO_2$ nanoparticles. The experiments were conducted based on the selected factors and their levels in Table 3. CNFs were dispersed in the mixing water by using a surfactant solution. After the dispersion, cement was added to the dispersions to get cementitious nanocomposites ready with water to cement ratio of 0.45 in accordance with ASTM 305. The morphology of the CNF Nanocomposites fracture surfaces was investigated using an ultra-high-resolution scanning electron microscope.

**Table 3** Optimum Combination and Replacement Levels for the Selected Nano-engineering Practices

| Mix Designs | C0T0 (control) | C0T3 | C0T5 | C2T0 | C4T0 | C2T3 | C4T3 | C2T5 | C4T5 |
|---|---|---|---|---|---|---|---|---|---|
| $TiO_2$ | 0 | 3 | 5 | 0 | 0 | 3 | 3 | 5 | 5 |
| CNF | 0 | 0 | 0 | 0.2 | 0.4 | 0.2 | 0.4 | 0.2 | 0.4 |

## Testing methods

**Fresh concrete tests:** The slump flow test was conducted in conformity with the standard techniques given by ASTM C143.[23] The slump flow test was carried out to evaluate the capabilities of $TiO_2$ and CNF in the slump retention. The density of the mixtures was obtained by weighing the fresh concrete into a standard mold with a specific volume in accordance with ASTM C 138 standard.[24]

**Strength tests:** The compressive strength test was conducted by using a hydraulic testing machine under the loading rate of 1300N/Sec at 3, 7, 28, 56, 90 and 180 days of curing in accordance with ASTM C39.[25] Cylindrical specimens with the diameter of 100 mm and the height of 200 mm were cast for splitting-tensile tests according to the ASTM C496.[26] Also, the flexural strength of concrete was obtained with using a simple beam with third-point loading in accordance with ASTM C78.[27] All the molds were covered with polyethylene sheets for 24 hours in the wet condition. Then the specimens were demolded and cured in water at a temperature of 20°C.

**Transport tests**: There are different methods to evaluate the absorption of concrete samples with $TiO_2$ and CNF. One is testing water absorption based on BS 1881-Part 122.[28] The cubic specimens were dried at 45°C for 14 days to reach the constant weight. Then samples were immersed in water and scaled after 0.5, 1, 24, 72 and 168 hours to measure the weight variation. This method would evaluate water absorption that happened in pores. These tiny voids are emptied by oven drying and occupied again with water after the immersion. In another approach, capillary absorption is measured through the non-saturated concrete specimens. In this method, a sample is in adjacent with a water layer on one lateral and absorbed water evaporation from the other part, a steady flowing regime through capillary absorption is established.[29] The test was performed for measuring of capillary water absorption in accordance with RILEM CPC 11.2, TC 14-CPC for testing capillary absorption of $TiO_2$ and CNF specimens. The cubic specimens with 100 mm dimensions were dried in the oven at 45±5°C. They were immersed in a water bath with 5 mm depth.

**Abrasion test:** Since the abrasion resistance of the cement paste is very slight compared to the aggregates, in this project it is aimed to explore the effect of $TiO_2$ and CNF on the increment of wear resistance of concrete. Meanwhile, as $TiO_2$ had no impact on the increment of wear resistance of concrete, rigid cement paste samples were used instead of concrete samples.[30] In this way, direct effects of nano $TiO_2$ and CNF on the abrasion resistance of cement paste were measured. One of the available test methods to this end is an accelerated loading test and rotary abrasion. The Hamburg-Wheel-Track (HWT), which employs a scaled dynamic wheel passing back and forth over the specimen, might simulate loading and wear of the applied coating. The mechanism of wear-out of the frictional resistance is at the heart of erosion analysis where such wear-out is a function of traffic, wet days and the shear strength of the sub base layer. A sliding and shearing type movement under the action of a rolling tire causes a load-induced shear stress $\tau$ that exceeds the effective shear strength of $TiO_2$ and CNF causing wear to take place. Testing will be conducted at room temperature under dry conditions, during which progress of surface rutting is monitored. A maximum acceptable rut depth of 6 mm at 20,000 passes is used in the specifications. Another approach for testing abrasion resistance is using a linear variable differential transformer (LVDT) to measure the depth into concrete surface created by a rotating diamond-core barrel attached to a drill press. The concrete surface abrasion resistance test is based on ASTM C944.[31] This test determines abrasion resistance of the surface concrete by measuring the weight loss of the concrete scratched by a rotating cutter in a given period. The cutter consists of a series of dressing wheels mounted on a rod that is attached to a drill press. Abrasion resistance tests were conducted on specimens cured under the same conditions. Surface abrasion resistance test for this research is performed on the surface of a 12-in diameter concrete cylinder. A drill press is used to apply a constant force through the cutter into the surface of specimens and to rotate the cutter at 200 revolutions per minute. In the research, a constant load of 22 lbs was applied on the drill press, and each test was performed for 10 minutes. A concrete specimen was measured before and at the end of an abrasion resistance test to determine the weight loss through the abrasion process.

**Freeze and thaw:** The resistance to freezing/thawing of $TiO_2$ and CNF samples was evaluated in accordance with ASTM C 666,[32] in which specimens were subjected to repeated freezing and thawing cycles. Specimens were used to measure the fundamental transverse frequency by using the force resonance method. Samples with dimensions of 100 × 100 × 400 mm were cured under standard conditions and tested for integrity by recording the relative dynamic modulus of elasticity (Eq. 1) every 25 cycles up to 300 cycles.

$$P_c = \frac{n_1^2}{n^2} \times 100$$

$P_c$: relative dynamic modulus of elasticity, after $c$ cycles of freezing/thawing (%)

$n$: the fundamental transverse frequency at zero cycles of freezing/thawing

$n_1$: the fundamental transverse frequency after $c$ cycles of freezing/thawing

## Bulk electrical resistivity

The bulk electrical resistivity was performed on water saturated concrete cylinders of 100×200 mm (4×8 in) in the lime water tank

after curing periods of 3, 28, 56, 90 and 180 days. Electrical resistivity is a function of moisture and electrolyte content of the pores in concrete, which measured based on AC impedance spectrometry using a resistance meter.[33] Experiments have been done with Wenner 4-probe meter. The likely difference and resulting current can be applied to find the electrical resistance. Three readings were obtained from the data logger for each cylinder specimen. The bulk resistivity was calculated as follows (Eq. 2):

$$\rho = \frac{V}{I} \times \left( A/L \right) = R \times \left( A/L \right)$$

Where $\rho$ is the electrical resistivity (KΩ cm), $R$ is bulk electrical resistance (KΩ), $A$ is a cross sectional area ($cm^2$), $L$ is the distance between two electrodes (cm), I is measured current, and V is the voltage.

**Shrinkage:** The shortening of concrete slabs might be caused by temperature decreases or moisture loss. After setting, concrete starts to shrink when water not used up by cement hydration, which is known as drying shrinkage. The shrinkage property of a concrete mixture can be determined by ASTM C 157.[34] This test method determines the change in length on drying of concrete bars which has been cured under the same curing condition. The lengths and weights at 1, 7, 14, 28, 56, 90-day age were recorded. Concrete mixtures were prepared in the laboratory and tested for their resistance to shrinkage cracking to evaluate the effectiveness of the $TiO_2$ and CNF were used.

**Mercury intrusion porosimetry (MIP):** The MIP has been one of the most commonly used methods to analyze the pore structure of porous materials; it involves evaluating the volume of mercury that is inserted into the sample. By using the principle of MIP, the pore size, connectivity and distribution of pores in CNF and $TiO_2$ samples can be calculated. To make the specimens for MIP measurement, the crushed samples were dried in an oven at about 110°C after 90 days of water curing and then tested by MIP to detect the pore volume based on the ASTM D 4284 standard.[35] The equation used for the calculation is the Washburn equation. The size of the air voids that are intruded is contrariwise proportional to the functional pressure.[36] Pore size ranges are measured based on a relationship between the amount of intruded mercury and the functional pressure. The equation between the pore size and functional pressure is commonly defined as follows (Eq. 3):

$$D = \frac{-4\gamma cos\theta}{P}$$

Where $D$ is the pore size (nm), $\gamma$ is the surface tension of mercury (dyne/cm), $\theta$ is the contact angle between solid and mercury (°) and $P$ is the functional pressure (Mpa).

# Results

## Fresh concrete tests

In this experimental program, rheological properties of nanoparticles were measured by the slump flow test. The slump flow measurements of all mixtures were in the range of 73-86 mm. The effects of $TiO_2$ and CNF on the flowability of mixtures are associated with the content of nanoparticles, as indicated in Figure 2. The slump flow test is a critical parameter to evaluate flow ability of concrete mixtures. The nanoparticles are shown to have several effects on the workability of concrete. As it indicated in Figure 2, the $TiO_2$ and CNF might lubricate solid particles of the cementitious materials and sand, which increases slump flow through the time. The lubrication effect is dominant after 30 minutes of the mixing process. Meanwhile, the nanoparticles captivate water and decrease flow ability. Another impact of using $TiO_2$ and CNF is keeping the rate of slump flow steady. Incorporating these nanomaterials generally made the concretes less viscous. The flowability characteristics of mixtures did not change significantly. Since applying CNF and $TiO_2$ might improve the consistency of concrete mixtures. Less bleeding and segregation were also found in the concrete mixtures containing both CNF and $TiO_2$.

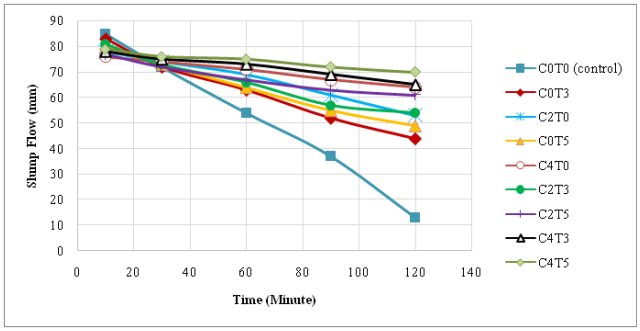


**Figure 2** Effect of $TiO_2$ and CNF content on flowability.

## Strength tests

The compressive, splitting-tensile and flexural strength of specimens up to 180 days are shown in Figures (3–5). It can be seen that the strength is developed in concretes containing nanoparticles in every mixture higher than that of control specimen. As it is shown in Figure 3, the compressive strength of concrete was meaningfully improved by using $TiO_2$ as a cementitious materials replacement. The 28-day compressive strength of concrete was heightened as much as 26.5% and 11.3% in comparison to that of the control specimen by replacing 3 and 5 wt% cement with $TiO_2$, respectively. The compressive strength increased from 26.5% to 52.4% when the 0.4 wt% CNF was added to the mixture. The growth in the compressive strength of concrete with nanoparticles compares to control concrete might be attributed to the pozzolanic reaction of $TiO_2$ and CNF. These kinds of reactions which are very effective based on pozzolanic performance, may lead to the development of the C-S-H gel.

Although $TiO_2$ would fill gel pores to grow the compressive strength, it has been found to decrease with the using $TiO_2$ from 3 wt% to 5 wt%. This compressive strength reduction might be attributed to applying too much $TiO_2$. After hydration activates, hydrate products diffuse and enclose $TiO_2$ as the kernel. If the amount and distance between these $TiO_2$ particles are suitable, the crystallization would be controlled to be a right state through restricting the growth of $Ca(OH)_2$ crystal by $TiO_2$. Since the cement matrix is much more compact, applying much $TiO_2$ is going to decrease the distance between nanoparticles. In this condition, crystallization of $Ca(OH)_2$ grows slightly and keep the ratio of crystal to C-S-H small. According to Figure 3, the compressive strength of concrete containing CNF is also improved. The 28-day compressive strength of concrete has been enhanced as much as 30.4% and 40.5% by replacing 0.2 wt% and 0.4 wt% of cement CNF. The increase in compressive strength can be attributed to the bridging effect of the CNFs for microcracks. The development of compressive strength containing CNF was also due to filler effect and the quick using of $Ca(OH)_2$ formed during hydration reactions of the cementitious materials. Compared $TiO_2$ with the CNF, the mixtures containing CNF had slightly higher compressive strength.

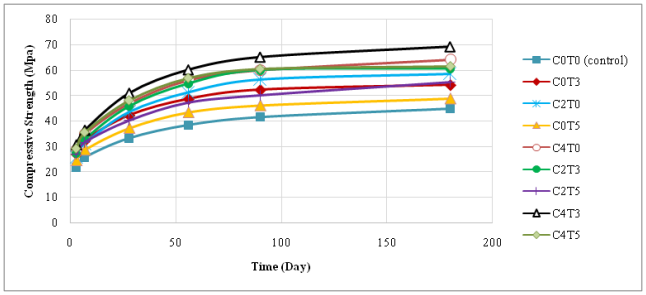


**Figure 3** Compressive strength of specimens.

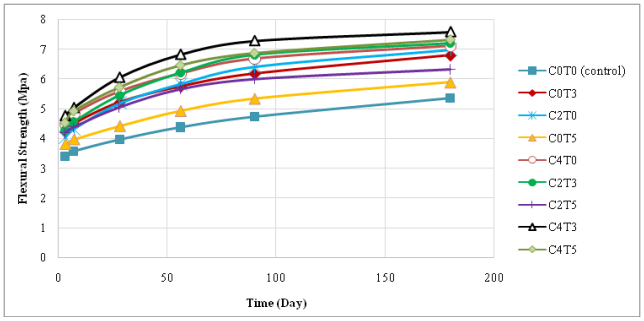


**Figure 4** Flexural strength of specimens.

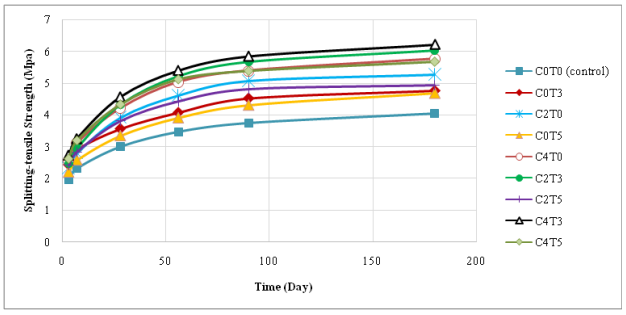


**Figure 5** Splitting-tensile strength of specimens.

Based on the results obtained from mixtures, flexural strength improvement in the $TiO_2$ and CNF mixtures is a significant and ascending trend can be observed in applying both nanoparticles at the same time. As it is shown in Figure 4, the addition of $TiO_2$ nanoparticles up to 3 wt% might lead to flexural strength growth, however, the addition of nanoparticles by 5 wt% results in lower flexural strength, meanwhile this is still higher than a control specimen. The reduced flexural strength may be explicated in different ways. This reduction in flexural strength by adding much $TiO_2$ nanoparticles might be due to the amount of $TiO_2$ existing in the mix is higher than the needed amount to mixed with the free lime during the process of the hydration. This might result in excess silica discharge and cause a strength shortage. The higher flexural strength in the mixtures containing CNF may be in the aftermath of the quick consumption of crystalline $Ca(OH)_2$. $TiO_2$ can contribute in the hydration process to generate C-S-H through reaction with $Ca(OH)_2$. CNF could recover the particle packing density and bridge the gel pores, which results in the volume of larger pores reduction. As it is shown in Figure 5, tensile strength trends are related to compressive strength developments, although this relationship depends on variations in the mix design. For evaluation of the $TiO_2$ and CNF influence, the higher this content is the greater, reducing the number of microcracks in the aggregate-paste interface that also increase the tensile strength. Furthermore, on growing the nanoparticles, the aggregate-paste transition zone is the weakest phase of the concrete. Tensile strength is a property that advances faster in the first days than compressive strength and it is much likely to have a higher hydration rate provided by $TiO_2$ promotes the former over the latter. Incorporating both $TiO_2$ and CNF at the same time not necessarily increase the strength. The decrease in strength could be due to the agglomeration and deficiencies caused by the dispersion of $TiO_2$ particles and CNF. When the amount of nanoparticles is significant, the fragile zone in the paste is going to increase, and it ends with a reduction in concrete strength.

## Transport tests

For measuring transport performance, the water absorption and capillary absorption of the concrete samples containing $TiO_2$ and CNF were measured at different time intervals. The results confirm that the percentage of water absorption and the height of capillary absorption are reduced by applying the $TiO_2$ and CNF nanoparticles. The performance of $TiO_2$ was slightly better than CNF in absorption. As it is shown in Table 4, increasing the curing time and percentages of nanoparticles may lead to a reduction in permeable gel pores due to the great bridging and filler effects of nanomaterials. The Interfacial Transition Zone (ITZ) in concrete is improved due to high reactivity as well as the filler effect of the $TiO_2$ nanoparticles. The total specific pore volumes of concretes are decreased.

**Table 4** Results of water absorption and capillary water absorption versus time

| No. | Mix design ID | Time (hr) | | | | | | | | | |
|---|---|---|---|---|---|---|---|---|---|---|---|
| | | 0.5 | 1 | 3 | 24 | 72 | 168 | 24 | 48 | 72 | 168 |
| | | Water absorption (%) | | | | | | Capillary water absorption (mm) | | | |
| 1 | C0T0 (control) | 2.45 | 3.3 | 4.17 | 4.61 | 4.95 | 5.32 | 2.75 | 4 | 5.15 | 5.68 |
| 2 | C0T3 | 1.98 | 2.85 | 3.78 | 4.21 | 4.61 | 5.01 | 2.33 | 3.52 | 4.69 | 5.32 |
| 3 | C0T5 | 1.62 | 2.53 | 3.35 | 3.8 | 4.26 | 4.58 | 1.92 | 3.13 | 4.24 | 4.81 |
| 4 | C2T0 | 2.32 | 3.15 | 4.05 | 4.39 | 4.76 | 5.13 | 2.64 | 3.82 | 4.91 | 5.43 |
| 5 | C4T0 | 1.86 | 2.69 | 3.6 | 3.94 | 4.39 | 4.74 | 2.19 | 3.34 | 4.46 | 4.96 |
| 6 | C2T3 | 1.73 | 2.56 | 3.33 | 3.81 | 4.24 | 4.51 | 2.1 | 3.23 | 4.31 | 4.84 |
| 7 | C4T3 | 1.66 | 2.57 | 3.28 | 3.75 | 4.1 | 4.44 | 1.96 | 3.16 | 4.22 | 4.71 |
| 8 | C2T5 | 1.55 | 2.41 | 3.19 | 3.52 | 3.92 | 4.29 | 1.85 | 3.05 | 4.1 | 4.63 |
| 9 | C4T5 | 1.36 | 2.28 | 3.12 | 3.57 | 3.98 | 4.35 | 1.73 | 2.91 | 3.95 | 4.58 |

## Abrasion test

Surface abrasion resistance test of this research was performed on the surface of a 12-in diameter concrete cylinder. Once the curing was finished after 72 hours, the abrasion resistance test was conducted on the surface to evaluate the effect of nanoparticles on the strength development of the surface concrete. The reason for performing this test was because it is a commonly known fact that as the strength of surface concrete increases, the resistance to abrasion also increases. As it is shown in Figure 6, utilizing 3 wt% $TiO_2$ had a lower abrasion weight loss rather than the control sample. The addition of $TiO_2$ up to 3 wt% reduced the mass loss values 30.52%. While, with adding more than 3 wt% $TiO_2$, abrasion resistance decreases slightly. The reason is attributed to the formation of a lump of nanoparticles in higher content and the supplementary cement replacement by nanomaterials might lead to enfeebling of the ITZ. Therefore, 5 wt% $TiO_2$ replacements even has much abrasion weight loss (9.95%) than the control sample. A lower weight loss of the abrasion test by increasing $TiO_2$ and CNF content indicates a higher strength of surface concrete, which is probably due to the pozzolanic reaction of $TiO_2$ and CNF. These kinds of reactions which are very effective based on pozzolanic performance, may lead to the development of the C-S-H gel. Depending on the results shown in Figure 6, incorporating CNF had much better results in comparison with $TiO_2$. The favorable result had obtained when both CNF and $TiO_2$ used together. C4T3 (4% CNF+3% $TiO_2$) showed the lowest abrasion weight loss, which was 54.64% less than the control sample. Figure 7 shows the measured rut depth and variation of different mixtures versus the number of wheel cycles. The data obtained from the HWT test. As shown in Figure 7, the rut depth for all specimens was less than 1 mm. Since the failure in the HWT test is defined for 6 mm rut depth in 20,000 cycles for flexible samples, the impact of $TiO_2$ and CNF was not visible distinctly. Therefore, all the mixtures provided accepted resistance to wear. Rut depth for samples with CNF was less than $TiO_2$, which indicates that CNF has much better performance rather than $TiO_2$. C4T3, C2T3, and C2T0 have shown most desirable abrasion resistance.

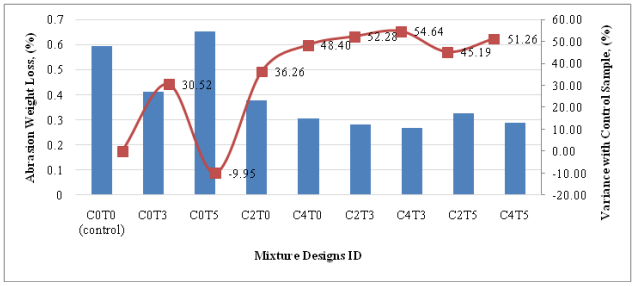


**Figure 6** Results of abrasion weight loss with using rotating cutter.

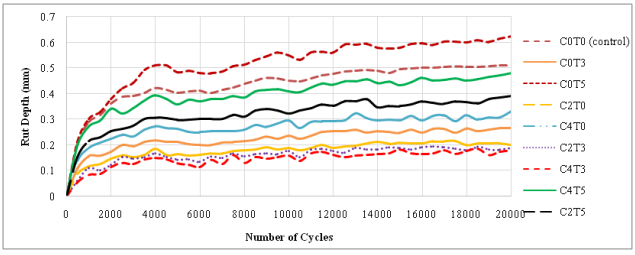


**Figure 7** Measured rut depth in the HWT test.

## Freeze and thaw

Visual observations indicated that honeycomb voids were found on specimens as freeze and thaw cycles continued and it caused the mass loss. The weight was recorded for all of the specimens during the freeze and thaw operations. One factor to evaluate the damage in concrete specimens subjected to the freeze and thaw cycles is a mass loss ratio. The relation between the mass loss ratio of different specimens is plotted in Figure 8. Dynamic modulus of the elasticity of the different mixture samples was measured at constant intervals up to 300 freeze and thaw cycles. As seen in Table 5, the mixtures with 3% and 5% $TiO_2$ displayed a slight decrease in the dynamic modulus of elasticity throughout the freeze and thaw test. Comparing to the initial condition of samples before freeze and thaw cycles, the control sample showed a decrease up to 38% in the dynamic modulus of elasticity at 300$^{th}$ cycles. While, the specimen with the 3% and 5% $TiO_2$ showed 5% and 15% decrease in the dynamic modulus of elasticity, respectively. The dynamic modulus of elasticity data is presented in Table 5. The relative dynamic modulus of elasticity is the ratio of the dynamic modulus at a specific interval, relative to the dynamic modulus at the start of the test. Figure 9 displays the relative dynamic modulus of elasticity data during the freeze and thaw cycles. The obtained data for specimens have been fitted to the likely function of the number of freeze and thaw cycles. The finest fits for samples have been acquired with a power equation (Eq. 4).

$$E_n / E_0 = k \times n^t$$

where $n$ is the number of freeze and thaw cycles and $k$ and $t$ are the coefficients. Table 6 summarizes all the test data on the dynamic modulus of elasticity and correlation coefficients.

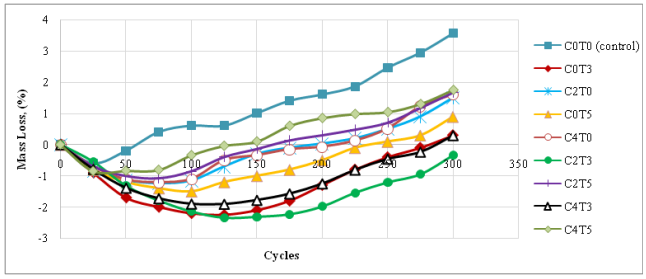


**Figure 8** Mass loss of concrete versus freeze and thaw cycles.

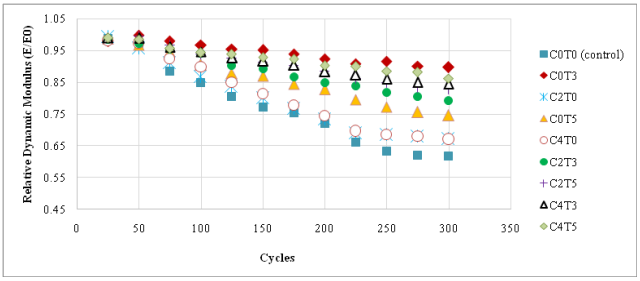


**Figure 9** Evolution of dynamic modulus of elasticity of concrete subjected to freeze and thaw cycles.

## Bulk electrical resistivity

The bulk electrical resistivity of concrete is a crucial factor that specifies the permeability of concrete to harmful agents. It has a significant correlation with the concrete microstructure, pore structure, and conductive ions. The bulk electrical resistivity results

for mixtures are shown in Figure 10. The values of all the samples were increased with the aging, principally in the initial days. This high rate increasing is attributed to hydration and hardening. The porosity of mixtures reduced gradually and the electrical resistivity growth decreased. It should be noted that the samples used in this evaluation were cured by keeping the samples in lime saturated water between test measurements. The results further show that for mixtures with nanoparticles, concrete resistivity was changed. The concrete mixtures with higher resistivities corresponding to using $TiO_2$ and CNF at the same time (at fixed w/c ratios). The bulk electrical resistivities of C4T3 and C2T3 were 45.8% and 39.3% higher than the control sample at the ages of 180 days, respectively. In accordance with Figure 10, the porosity of concrete relatively decreased with the incorporating nanoparticles at the same water-binder ratio. It was also observed that concretes produced with $TiO_2$ had a lower bulk electrical resistivity to those of having CNF. According to the obtained results of the water absorption in Table 4, the high values of CNF mixtures were expected due to the much lower water absorption capacity in comparison to control sample.

**Table 5** Dynamic modulus of concrete after the particular freeze and thaw cycles (Gpa)

| No. | Mix designs | Freeze and thaw cycles | | | | | | | | | | | |
|---|---|---|---|---|---|---|---|---|---|---|---|---|---|
| | | 25 | 50 | 75 | 100 | 125 | 150 | 175 | 200 | 225 | 250 | 275 | 300 |
| 1 | C0T0 (control) | 37.23 | 36.08 | 32.98 | 31.63 | 30.02 | 28.78 | 28.1 | 26.82 | 24.65 | 23.57 | 23.14 | 22.97 |
| 2 | C0T3 | 41.15 | 41.03 | 40.31 | 39.83 | 39.27 | 39.14 | 38.67 | 37.98 | 37.37 | 37.71 | 37.09 | 36.89 |
| 3 | C0T5 | 40.04 | 38.71 | 37.91 | 36.21 | 35.13 | 34.82 | 33.83 | 33.1 | 31.84 | 30.93 | 30.22 | 29.81 |
| 4 | C2T0 | 39.37 | 37.61 | 35.83 | 34.1 | 32.9 | 31.43 | 30.12 | 28.82 | 27.15 | 26.93 | 26.71 | 26.42 |
| 5 | C4T0 | 39.13 | 38.06 | 36.11 | 35.13 | 33.23 | 31.83 | 30.43 | 29.1 | 27.21 | 26.82 | 26.62 | 26.22 |
| 6 | C2T3 | 44.54 | 43.32 | 42.54 | 41.88 | 40.22 | 39.72 | 38.62 | 37.78 | 37.37 | 36.41 | 35.82 | 35.33 |
| 7 | C4T3 | 43.41 | 42.49 | 41.22 | 40.61 | 39.82 | 39.31 | 38.8 | 37.92 | 37.5 | 36.92 | 36.51 | 36.32 |
| 8 | C2T5 | 38.79 | 38.63 | 37.51 | 36.41 | 35.93 | 35.4 | 34.98 | 34.32 | 33.41 | 32.9 | 32.33 | 32.11 |
| 9 | C4T5 | 38.05 | 37.52 | 36.43 | 35.92 | 35.7 | 35.33 | 35.11 | 34.34 | 34.26 | 33.7 | 33.56 | 32.83 |

**Table 6** Dynamic modulus of elasticity correlation coefficients

| No. | Mixture design | k | t | $R_2$ | The Decrease in dynamic modulus of elasticity (%) |
|---|---|---|---|---|---|
| 1 | C0T0 (control) | 2.18 | -0.214 | 0.919 | 38.3 |
| 2 | C0T3 | 1.19 | -0.049 | 0.903 | 10.28 |
| 3 | C0T5 | 1.57 | -0.124 | 0.912 | 25.54 |
| 4 | C2T0 | 1.91 | -0.181 | 0.934 | 32.84 |
| 5 | C4T0 | 1.96 | -0.183 | 0.905 | 32.97 |
| 6 | C2T3 | 1.43 | -0.099 | 0.915 | 20.69 |
| 7 | C4T3 | 1.32 | -0.076 | 0.951 | 15.42 |
| 8 | C2T5 | 1.36 | -0.083 | 0.904 | 17.15 |
| 9 | C4T5 | 1.23 | -0.058 | 0.937 | 13.72 |

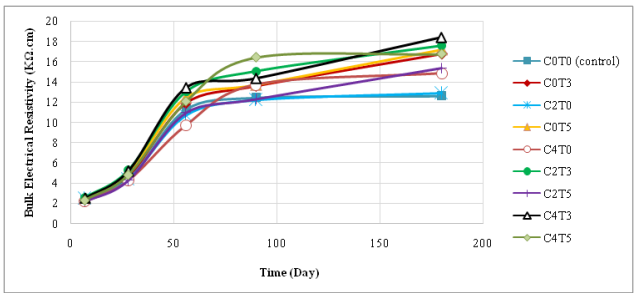


**Figure 10** Bulk resistivity of different mixtures of all ages.

## Shrinkage

The outcomes of shrinkage test are presented in Figure 11. It was observed that there was a direct relationship between the values of free shrinkage and amount of nanoparticles in the concrete. It can be pointed out that samples had high shrinkage at first initial hours and this rate decreased slightly by time. The reduction shrinkage in nanoparticles is accredited to microstructure. When excess water begins to evaporate from the concrete's surface after setting, an air/water interface is set up within the capillary pores of the paste. Due to high surface tension, stress induced on the internal walls of the slight pores. This stress is an inward pulling force that inclines to close up the pore structures and decrease the volume of the capillaries. As much as these capillary pores are high, concrete has much potential to shrink. Therefore, using nanoparticles is the main reason for decreasing capillary void content and surface tension effects and consequently reducing the shrinkage as water evaporates from within the concrete. As expected, control sample had the highest shrinkage among other mixtures. The performance of CNF in controlling shrinkage was better than $TiO_2$. However, the largest shrinkage values were recorded for the mixture that contains CNF at first hours. The reason is attributed to free shrinkage which occurred between 4 and 6 hours. The shrinkage began long before the occurrence of the phenomena that determine a change in the pseudo-rigid structure of the mixture. This shrinkage decreased gradually. In C4T0, 47% reduction was observed in shrinkage at 90 days. The nanoparticles addition in the mixture results in lower shrinkage values.

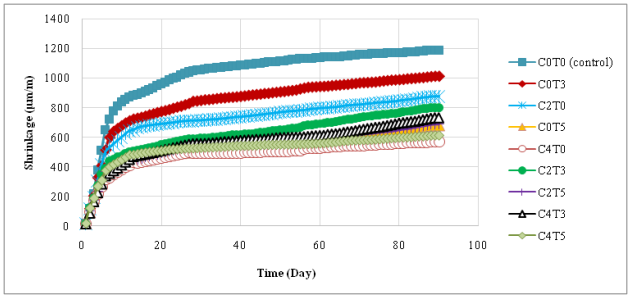


**Figure 11** Results of shrinkage test.

## Mercury intrusion porosimetry (MIP)

The pore size distribution of concretes is shown in Table 7. In this study, the pore structure parameters such as total specific pore volume and pore size distribution are calculated. Based on pore size impacts on concrete performance, the pore size in concrete is categorized into four classes: harmless pore (<20 nm), few-harm pore (20–50 nm), harmful pore (50–200 nm) and multi-harm pore (>200 nm).[37] One of the results obtained from MIP analysis was an addition of nanoparticles increase the amounts of harmless pores and reduce the amounts of harmful pores. This change improved the density of concretes and pore structure. The effectiveness of CNF in improving the pore structure is much better than $TiO_2$. The total amount of the harmless in mixtures containing CNF was increased to the largest extent. Nanoparticles are dispersed in concrete with a certain distance from each other. By initiation of hydration, hydrate products diffuse in the paste and encircle nanoparticles. The crystallization depends on the nanoparticles and it impacts the $Ca(OH)_2$ development. This reaction might promote cement hydration due to the high activity of nanoparticles such as $TiO_2$ and CNF. Although using nanoparticles makes the matrix more consistent, increasing too much of nanoparticles might have severe effects. The reason is attributed to a limitation in enough growing up of crystal quantity. As shown in Table 7, the addition of CNF and nano $TiO_2$ reduced the total specific pore volumes of concretes.

**Table 7** Total specific pore volumes and Pore size distribution of mixtures

| No. | Mixture design | Total specific pore volume (ml/g) | Pore size distribution (ml/g (%)) | | | |
|---|---|---|---|---|---|---|
| | | | Harmless pores (<20 nm) | Few-harm pore (20–50 nm) | Harmful pore (50–200 nm) | Multi-harm pore (>200 nm) |
| 1 | C0T0 (control) | 0.0407 | 0.0064 | 0.0103 | 0.0151 | 0.0089 |
| 2 | C0T3 | 0.0374 | 0.0061 | 0.0114 | 0.0128 | 0.0071 |
| 3 | C0T5 | 0.0319 | 0.006 | 0.0125 | 0.0069 | 0.0065 |
| 4 | C2T0 | 0.0382 | 0.0063 | 0.0121 | 0.0121 | 0.0077 |
| 5 | C4T0 | 0.0349 | 0.0061 | 0.0133 | 0.0084 | 0.0071 |
| 6 | C2T3 | 0.0355 | 0.0062 | 0.0123 | 0.0102 | 0.0068 |
| 7 | C4T3 | 0.0331 | 0.0061 | 0.0137 | 0.0069 | 0.0064 |
| 8 | C2T5 | 0.0296 | 0.006 | 0.0135 | 0.0043 | 0.0058 |
| 9 | C4T5 | 0.0289 | 0.0061 | 0.0129 | 0.0042 | 0.0057 |

## Conclusion

I. The effects of $TiO_2$ and CNF on the flowability of mixtures are associated with the content of nanoparticles. These nanomaterials lubricate solid particles of the cementitious materials and sand, which increases slump flow through the time and keep it at the constant rate with no significant change. Besides, consistency of concrete mixtures has been improved.

II. The compressive, splitting-tensile and flexural strength of specimens are developed in concretes containing nanoparticles due to the pozzolanic reaction of $TiO_2$ and CNF. These kinds of reactions which are very effective based on pozzolanic performance, may lead to the development of the C-S-H gel.

III. Although $TiO_2$ would fill gel pores of the paste to improve pore structure, using too much $TiO_2$ decrease strength. After hydration activates, hydrate products diffuse and enclose $TiO_2$ as akernel. Applying much $TiO_2$ is going to reduce the distance between nanoparticles. In this condition, crystallization of $Ca(OH)_2$ grows slightly and keep the ratio of crystal to C-S-H small.

IV. Concrete containing CNF is also improved in mechanical properties. It can be attributed to the bridging effect of the CNFs for microcracks and filler effect. Compared $TiO_2$ with the CNF, the mixtures containing CNF had slightly higher compressive strength. CNF could recover the particle packing density and bridge the gel pores, which results in the volume of larger pores reduction.

V. Incorporating both $TiO_2$ and CNF at the same time not necessarily increase the strength. The decrease in strength could be due to the agglomeration and deficiencies caused by the dispersion of $TiO_2$

particles and CNF. When the amount of nanoparticles is significant, the fragile zone in the paste is going to increase and it ends with a reduction in concrete strength.

VI. The results confirm that the percentage of water absorption and the height of capillary absorption are reduced by applying the $TiO_2$ and CNF nanoparticles. The performance of $TiO_2$ was slightly better than CNF in absorption. The ITZ in concrete is improved due to high reactivity as well as a filler effect of the $TiO_2$ nanoparticles. The total specific pore volumes of concretes are decreased.

VII. Utilizing 3 wt% $TiO_2$ had a lower abrasion weight loss rather than the control sample. While adding more than 3 wt% $TiO_2$ decreased abrasion resistance slightly due to the formation of a lump of nanoparticles. Higher content of the supplementary cement replacement by nanomaterials might lead to enfeebling of the ITZ.

VIII. Based on data from the HWT, the rut depth for all specimens was less than 1 mm. Therefore, the HWT test was not a suitable procedure to show the impact of $TiO_2$ and CNF distinctly.

IX. The mixtures with 3% and 5% $TiO_2$ displayed a slight decrease in the dynamic modulus of elasticity throughout the freeze and thaw test (5% and 15%, respectively).

X. Bulk electrical resistivity had a great correlation with the concrete microstructure. The values of all the samples were increased with the aging, mainly in the initial days due to hydration and hardening. The concrete mixtures with higher resistivities corresponding to using $TiO_2$ and CNF at the same time. Concrete produced with $TiO_2$ had a lower bulk electrical resistivity to those of had CNF.

XI. The reduction shrinkage in nanoparticles is accredited to microstructure. The performance of CNF in controlling shrinkage was better than $TiO_2$. However, the largest shrinkage values were recorded for the mixture that contains CNF at opening hours due to free shrinkage. The nanoparticles addition in the mixture results in lower shrinkage values.

XII. The addition of nanoparticles increases the amounts of harmless pores and reduces the amounts of harmful pores. The effectiveness of CNF in improving the pore structure is much better than $TiO_2$. The total numbers of the harmless in mixtures containing CNF were increased to the largest extent.

## Acknowledgements

None.

## Conflicts of interest

The author declares there is no conflict of interest.

## References

1. Sihai Wen, DDL Chung. Enhancing the Seebeck Effect in Carbon Fiber Reinforced Cement by Using Intercalated Carbon Fibers. *Cem Concr Res*. 2000;30(8):1295–1298.
2. Sihai Wen, DDL Chung. Electrical Behavior of Cement-Based Junctions Including the pn-Junction. *Cem Concr Res*. 2001;31(1):129–133.
3. Jingyao Cao, DDL Chung. Effect of Strain Rate on Cement Mortar under Compression, Studied by Electrical Resistivity Measurement. *Cem Concr Res*. 2002;32(5):817–819.
4. H Li, MH Zhang JP Ou. Abrasion resistance of concrete containing nanoparticles for pavement. *Wear J*. 2006;260(11–12):1262–1266.
5. H Li, MH Zhang, JP Ou. Flexural fatigue performance of concrete containing nano-nanoparticles for pavement. *Int J Fatigue*. 2007;29:1292–1301.
6. MJ Hanus, AT Harris. Nanotechnology innovations for the construction industry. *Prog Mater Sci*. 2013;58(7):1056–1102.
7. F Wang, L Yang, G Sun, L Guan, S Hu. The hierarchical porous structure of substrate enhanced photocatalytic activity of TiO2/cementitious materials. *Constr Build Mater*. 2014;64:488–495.
8. Lu Yang, Fazhou Wang, Dan Du, et al. Enhanced photocatalytic efficiency and long-term performance of $TiO_2$ in cementitious materials by activated zeolite fly ash bead carrier. *Construction and Building Materials*. 2016;126:886–893.
9. Berdahl P, Akbari H. *Evaluation of titanium dioxide as a photocatalyst for removing air pollutants*. California Energy Commission, PIER Energy-Related Environmental Research program, CEC-500-2007-112. 2008.
10. Beeldens A. *An environmentally friendly solution for air purification and self-cleaning effect: the application of $TiO_2$ as photocatalyst in concrete*. In: Proceedings of transport research arena Europe, TRA, Göteborg, Sweden. 2006.
11. Z Li, B Gao, GZ Chen, et al. Carbon nanotube/titanium dioxide (CNT/TiO2) core–shell nanocomposites with tailored shell thickness, CNT content and photocatalytic/photoelectrocatalytic properties. *Appl Catal B-Environ*. 2011;110: 50–57.
12. Q Xiang, J Yu, M Jaroniec. Graphene-based semiconductor photocatalysts. *Chem Soc Rev*. 2002;41(2):782–796.
13. J Ryu, S Kim, HI Kim, et al. Self-assembled $TiO_2$ agglomerates hybridized with reduced-graphene oxide: A high-performance hybrid photocatalyst for solar energy conversion. *Chem Eng J*. 2015;262:409–416.
14. HI Kim, S Kim, JK Kang, et al. Graphene oxide embedded into $TiO_2$ nanofiber: Effective hybrid photocatalyst for solar conversion. *J Catal*. 2014;309:49–57.
15. M Inagaki, Y Yang, F Kang. Carbon Nanofibers Prepared via Electrospinning. *Adv Mater*. 2012;24(19):2547–2566.
16. HQ Hou, DH Reneker. Carbon Nanotubes on Carbon Nanofibers: A Novel Structure Based on Electrospun Polymer Nanofibers. *Adv Mater*. 2004;16(1):69–73.
17. J Mu, C Shao, Z Guo, et al. High Photocatalytic Activity of ZnO-Carbon Nanofiber Heteroarchitectures. *ACS Appl Mater Interfaces*. 2011;3(2):590–596.
18. W Guo, F Zhang, C Lin, et al. Direct Growth of $TiO_2$ Nanosheet Arrays on Carbon Fibers for Highly Efficient Photocatalytic Degradation of Methyl Orange. *Adv Mater*. 2012;24(35):4761–4764.
19. S Kim, M Kim, YK Kim, et al. Core-shell-structured carbon nanofiber-titanate nanotubes with enhanced photocatalytic activity. *Appl Catal B-Environ*. 2014;148–149:170–176.
20. S Kim, SK Lim. Preparation of $TiO_2$-embedded carbon nanofibers and their photocatalytic activity in the oxidation of gaseous acetaldehyde. *Appl Catal B-Environ*. 2008;84(1–2):16–20.
21. ASTM C150/C150M-16e1. *Standard Specification for Portland Cement*. ASTM International, West Conshohocken, PA, USA. 2016.
22. ASTM C33/C33M-16. *Standard Specification for Concrete Aggregates*. ASTM International, West Conshohocken, PA, USA. 2016.
23. ASTM C143/C143M-15a. *Standard Test Method for Slump of Hydraulic-Cement Concrete*. ASTM International, West Conshohocken, PA, USA. 2015.
24. ASTM C138/C138M-16a. *Standard Test Method for Density (Unit*

*Weight), Yield, and Air Content (Gravimetric) of Concrete*. ASTM International, West Conshohocken, PA, USA. 2016.

25. ASTM C39/C39M-16b. *Standard Test Method for Compressive Strength of Cylindrical Concrete Specimens*. ASTM International, West Conshohocken, PA, USA. 2016.
26. ASTM C496/C496M-11. *Standard Test Method for Splitting Tensile Strength of Cylindrical Concrete Specimens*. ASTM International, West Conshohocken, PA, USA. 2004.
27. ASTM C78/C78M-16. *Standard Test Method for Flexural Strength of Concrete (Using Simple Beam with Third-Point Loading)*. ASTM International, West Conshohocken, PA, USA. 2016.
28. BS 1881–116. *Testing concrete*. Method for determination of compressive strength of concrete cubes, USA. 1983.
29. D Perraton, PC Aïtcin, *A Carles-Gbergues*. Permeability, as seen by the researcher, In: Y Malier editor. High Performance Concrete: From Material to Structure, E & FN Spon, London, UK, 1994. p. 186–195.
30. Hassan MM, Dylla H, Mohammad LN, et al. Evaluation of the durability of titanium dioxide photocatalyst coating for concrete pavement. *Constr Build Mater*. 2010;24(8):1456–1461.
31. ASTM C944/C944M-12. *Standard Test Method for Abrasion Resistance of Concrete or Mortar Surfaces by the Rotating-Cutter Method*. ASTM International, West Conshohocken, PA, USA. 2012.
32. ASTM C666/C666M-15. *Standard Test Method for Resistance of Concrete to Rapid Freezing and Thawing*. ASTM International, West Conshohocken, PA, USA. 2015.
33. P Gu, P Xie, JJ Beaudoin, et al. AC impedance spectroscopy (II): microstructural characterization of hydrating cement–silica fume systems. *Cem Concr Res*. 1992;23(1):157–168.
34. ASTM C157/C157M-08e1. *Standard Test Method for Length Change of Hardened Hydraulic-Cement Mortar and Concrete*. ASTM International, West Conshohocken, PA, USA. 2014.
35. ASTM D4284-12e1. *Standard Test Method for Determining Pore Volume Distribution of Catalysts and Catalyst Carriers by Mercury Intrusion Porosimetry*. ASTM International, West Conshohocken, PA, USA. 2017.
36. L Tang, LO Nilsson. Rapid determination of chloride diffusivity of concrete by applying an electric field. *ACI Mater J*. 1992;89(1):49–53.
37. Q Ye. The study and development of the nano-composite cement structure materials. *New Build Mater*. 2001;1:4–6.

**Citation:** Joshaghani A. Evaluating the effects of titanium dioxide (TiO2) and carbon-nanofibers (CNF) as cement partial replacement on concrete properties. *MOJ Civil Eng.* 2018;4(1):29–38. DOI: 10.15406/mojce.2018.04.00094